Three-dimensional assessments are necessary to determine the true spatial tissue composition of diseased tissues

André Forjaz[1+], Eduarda Vaz[1+], Valentina Matos Romero[1], Saurabh Joshi[1], Alicia M. Braxton[2], Ann C. Jiang[3], Kohei Fujikura[4], Toby Cornish[5], Seung-Mo Hong[6], Ralph H. Hruban[7,8], Pei-Hsun Wu[1,9], Laura D. Wood[7,8], Ashley L. Kiemen [7,8,9*], and Denis Wirtz[1,7,8,9*]

[1]Department of Chemical & Biomolecular Engineering, Johns Hopkins University, Baltimore, MD

[2]Department of Comparative Medicine, Medical University of South Carolina, Charleston, SC

[3]Department of Biomedical Engineering, Johns Hopkins University, Baltimore, MD

[4]Department of Medical Genetics, Life Sciences Institute, University of British Columbia, Vancouver, BC, Canada

[5] Department of Pathology, University of Colorado School of Medicine, Aurora, CO

[6]Department of Pathology, Asan Medical Center, University of Ulsan College of Medicine, Seoul, Republic of Korea

[7]Department of Pathology, The Sol Goldman Pancreatic Cancer Research Center, Johns Hopkins School of Medicine, Baltimore, MD[8]Department of Oncology, Johns Hopkins School of Medicine, Johns Hopkins University, Baltimore, MD

[9]The Johns Hopkins Institute for NanoBioTechnology, Johns Hopkins University, Baltimore, MD

+ Authors contributed equally

***Send correspondence to:**

Denis Wirtz, Ph.D.
Croft 130
Department of Chemical & Biomolecular Engineering
3400 N Charles St, Baltimore MD, 21218
wirtz@jhu.edu

Ashley Kiemen, Ph.D.
Pathology 142
Department of Pathology
600 N Wolfe St, Baltimore, MD 21287
kiemen@jhmi.edu

Conflict of interest statement

The authors declare no conflicts of interest.

Sources of Support

The authors acknowledge the following sources of support: U54CA268083, and UG3CA275681 grants from the National Cancer Institute; Lustgarten Foundation-AACR Career development award for pancreatic cancer research in honor of Ruth Bader Ginsburg; Susan Wojcicki and Denis Troper; The Carl and Carol Nale Fund for Pancreatic Cancer Research; Rolfe Pancreatic Cancer Foundation.

ABSTRACT

Methods for partially resolved cellular profiling has enabled in-depth quantitative tissue mapping via thinly cut sections to study inter-patient and intra-patient differences in normal human anatomy and disease onset and progression. These methods often profile extremely limited spatial regions, which may impact the evaluation of heterogeneity due to tissue sub-sampling**.** Here, we applied CODA, a deep learning-based tissue mapping platform, to reconstruct the 3D microanatomy of surgically resected human pancreas biospecimens obtained from patients diagnosed with pancreatic cancer. To compare differences in the inter- and intra-tumoral heterogeneity, we assessed the bulk and spatially resolved tissue composition of a cohort of two-dimensional (2D) whole slide images (WSIs), and a cohort of 3D serially sectioned and reconstructed tissues of pancreata. Here, we show the strength of using 3D as the gold standard, by measuring the information loss and sampling problems when using WSIs and TMAs. We demonstrate that spatial correlation in microanatomical tissue content decays significantly within a span of just a few microns within tumors. As a corollary, hundreds of TMAs and tens of WSIs are required to estimate spatial bulk tumor composition with <10% error in any given pancreatic tumor. In sum, we demonstrate that 3D assessments are necessary to accurately assess tumor burden and tissue composition. These preliminary results show the importance of rate of sampling necessary to more reliably assess spatially resolved tissue composition.

INTRODUCTION

Recent development in numerous spatial profiling technologies has led to an array of projects aimed at the construction of atlases to quantitatively explore the spatial heterogeneities in cell and tissue compositions, architecture, as well as the epigenomic, proteomic, and metabolomic landscapes of tissue regions, whole organs, and even whole organisms.[1–9] These assays have helped identify, for instance, changes in cellular composition during development, aging and the progression of diseases such as cancer and cardiovascular disease. The majority of measurements of spatial cellular composition are typically conducted using just one or a very limited number of thin tissue sections. Due to technical and financial limitations, current spatial transcriptomic and proteomic methods to map the local cellular composition - CODEX, IMC, Visium, DBitseq, seqFISH, MERFISH, etc. - are designed to function on tissue sections of small area.[1,6,10–13]

For a histological section of standard thickness 5 µm, a 1-mm^2 core in a tissue microarray (TMA) represents a volume of tissue of just 0.005 mm^3, while a spatial 11 x 11 mm^2 transcriptomic assessment using standard spatial transcriptomics (e.g. Visium) corresponds to a tissue volume of 0.6 mm^3. The volumes sampled by spatial omics techniques represent a minuscule fraction of the volume of human organs and diseased tissues, with regions of deep profiling representing as little as one one-millionth of the volume of a diseased tissue. More standard techniques, including the gold standards of diagnostic anatomic pathology, hematoxylin and eosin (H&E) and immunohistochemistry (IHC), make use of whole microslides.[14,15] These slides feature a lateral size of 2 x 5 cm^2, corresponding to a volume of 5 mm^3, which allows for the collection of whole slide images (WSIs), corresponding to 10 and 1,000 times the volumes of a section for transcriptomic assessment and a standard TMA core, respectively. Hence, while these technologies represent a major advance in our ability to profile tissue, cellular, and sub-cellular structures, we must consider their limitations caused by potential under-sampling of tissues.[16]

The implicit assumption of limited sampling provided by TMAs and WSIs is that the phenotypes of cells and their respective locations, associated density, and spatial correlations found in the sampled region are representative of those in the 3D tissue from which the TMA core or the whole slide was collected. This may not present a major issue for common pathological assessments (using whole slides) that address binary questions, such as the absence/presence of tumor cells or inflammation. In clinic patient settings, 2D assessments have proved to be typically sufficient.

New work has demonstrated the utility of tissue clearing and serial sectioning-based approaches to create quantifiable volumes of human tissues and tumors to assess microanatomical maps of volumes of tissue of >1 cm^3 at cellular resolution. [17–23] Here, we use the recently developed 3D imaging workflow CODA to assess the spatial composition of key types of cells in large volumes (>1cm^3) of human pancreas containing pancreatic ductal adenocarcinoma (PDAC), the deadliest form of pancreatic cancer.[19] CODA aligns 100's-1000's of serial tissue sections with high resolution, automatically annotates tissue components in H&E sections using deep learning semantic segmentation, deconvolves H&E channels to identify individual cells, and reconstructs 3D maps of the tissue sample.[19] Armed with these 3D maps, we determine the minimum number of TMA-sized and microslides necessary to reach a preset percentage error in the assessment of the true spatially resolved and bulk tissue compositions of that 3D diseased tissue.

We find that 2D sampling – using one or just a few TMA cores or WSIs – is typically insufficient in the determination of tissue composition or tumor burden, or the selection of regions of interest for creation of TMA cores and capturing rare small events such as small cluster of cancer cells in a tumor.[24] We show

that sections inside a tumor, sometimes just tens of microns from each other, will have completely different, uncorrelated contents in cellular and non-cellular components. 2D assessments of "representative" slides have shown to particularly fail at detecting rare events, such as PDAC content in tumor with low PDAC burden.[20,24]

This work aims at studying the impact of tissue sampling when studying malignant tissues. Sets 3D tumor pathology as the gold standard at mitigating intra-tissue variability, and studies the loss of information when using other pathology assessments, such as WSIs and TMAs.

METHODS

Pancreas specimen acquisition

This retrospective study was approved by the Johns Hopkins University Institutional Review Board (IRB). Three cohorts of pancreas tissue were assembled here, which we term TMA, 2D-WSI, and 3D-CODA. The tissue microarray TMA was purchased from TissueArray. It contained 80 1.5 mm diameter cores taken from the pancreata of 40 individuals diagnosed with pancreatic cancer. The 2D WSI cohort contained tissue from the pancreata of 64 individuals who underwent surgical resection for pancreatic cancer at the Johns Hopkins Hospital, and is a cohort that was previously published.[25] The 3D pancreas cohort contained tissue from the pancreata of seven individuals who underwent surgical resection for pancreatic cancer at the Johns Hopkins Hospital, and is a cohort that was previously published. [18,19]

Tissue processing

Resected tissues were formalin-fixed, paraffin embedded, and sectioned at a thickness of 4 µm. For the TMA and 2D-WSI cohorts, a single histological section was stained with H&E. For the 3D-CODA cohort, a minimum of 270 serial sections were taken, and every third section was stained with H&E, for a minimum of 90 H&E-stained tissue sections per sample. H&E-stained images were digitized at 20x magnification using a Hamamatsu S360 scanner.

Segmentation of pancreatic microanatomy in 2D

A previously developed deep learning semantic segmentation pipeline for the labelling of distinct microanatomical components in histological images was adapted here to label ten microanatomical components of human pancreatic cancer histology at 1 µm per pixel resolution: pancreatic cancer, pancreatic cancer precursor lesions, normal ductal epithelium, acinar tissue, islets of Langerhans, vasculature, nerves, fat, and stroma.[19,26] Convolutional neural networks were trained in MATLAB2023b to classify the TMA cores, 2D-WSI, and 3D-CODA cohorts of tissues. Manual annotations of the ten microanatomical tissue components were generated on a subset of histological images, and fed into the CODA-segmentation workflow for retraining of a resnet-50 network. Resulting networks were deemed acceptable if the overall accuracy exceeded 90% and minimum per-class precision and recall exceeded 85%.

Reconstruction of pancreatic microanatomy in 3D

CODA image registration was used to create digital tissue volumes from the serial H&E images for the seven samples in the 3D-CODA cohort.[19] This nonlinear registration workflow iteratively aligns serial stacks of images (with the reference coordinates at the center of the stack), and utilizes a two-step global and local calculation in MATLAB2023b. Images are downsampled to a resolution of eight µm per pixel, converted to greyscale, and Gaussian-filtered. Global registration angle is calculated through maximization of the cross correlation of radon-transforms of the filtered images taken at discrete angles from 0 - 360°, and registration translation is calculated through maximization of the cross correlation of

the rotated, filtered images. Local registration is computed by repeating this process along subsampled regions of the two globally registered images. This registration is repeated for all images in the serial samples and is subsequently rescaled and applied to the high resolution (1 µm per pixel resolution) H&E and microanatomically segmented H&E images.

Calculation of variation in tissue composition in 2D and 3D

For each discrete sample in the TMA, 2D-WSI and 3D-CODA cohort, overall microanatomical composition was assessed. First, the number of pixels classified as each of the 10 microanatomical tissue types segmented by the deep learning model was determined. Next, composition was defined as the area percent of each tissue type in each sample. Variation in tissue composition in the 2D-WSI cohort was defined as the distribution of composition of each tissue type segmented by the deep learning model. Variation in tissue composition in the 3D-CODA cohort was defined as the distribution of composition of each tissue type along the z-dimension of the serial stack of images, taking each serial histological image as an independent measurement. Minimum, maximum, mean, median, standard deviation, and histogram bin counts of each tissue component composition in the 2D-WSI and 3D-CODA cohorts were determined. In determination of the distribution of tissue composition in the 3D-CODA cohort, samples containing >90 serial images were randomly subsampled to contain 90 consecutive images.

Calculation of the number of tissue microarrays necessary to understand WSI and 3D tissue composition

Virtual TMAs (vTMAs) were generated in the 2D-WSI and 3D-CODA samples. First, a 2D or 3D coordinate was generated. Pixels were extracted corresponding to a 1 x 1 mm^2 square surrounding the coordinates. A circular filter was applied to this extracted square to leave a 1-mm diameter disk representing a vTMA taken from the 2D or 3D image. To determine the number of vTMAs necessary to accurately estimate the tissue composition of a WSI or 3D pancreatic cancer tissue sample, random coordinates were determined, virtual TMAs were generated, and the tissue composition of each vTMA was recorded. Error was calculated between the per-class vTMA tissue composition and the overall composition of the WSI or 3D tissue sample. Another random vTMA was generated, added to the first vTMA, and error was recalculated for the combined sampling of two vTMAs. This process was repeated for sampling of up to 200 vTMAs. One thousand such simulations were performed to determine the general trend of per-class TMA error in assessment of WSI and 3D sample tissue composition.

Calculation of the decay in spatial correlation within 2D and 3D samples

In each sample of the 3D-CODA cohort, 2D planes of pixels were extracted from each classified tissue volume. For each segmented tissue component, the cross-correlation of the pixels classified as that component in that plane to all other planes of the 3D-sample was determined, and this correlation along with the distance between the planes was recorded. This process was repeated for all possible combinations of planes containing in each image, and was repeated for each of the seven tissue samples. Aggregate correlation of composition of a single tissue component as a function of distance within a 3D

sample was defined as the mean cross-correlation of that tissue component across all images of all samples.

Calculation of the change in tissue composition along vTMA cores

Change in tissue composition along serial sections of a vTMA core was determined. First, manual selection of coordinates on the first image of a sample was selected corresponding to a region visibly seen to contain invasive cancer. Next, a virtual core was extracted from the 3D segmented tissue volume corresponding to a cylinder of 1 mm diameter. Serial vTMAs were taken from each core, and the tissue composition of each serial vTMA was determined. Error in composition of each tissue type between the initial, manually selected vTMA and each serial TMA was calculated, and recorded along with the section number of that virtual serial TMA.

Calculation of the number of sections necessary to understand tumor burden

Tumor burden was defined in two ways. For pancreatic cancer precursor lesions, PanIN burden was defined as the volume of PanIN normalized by the combined volume of PanIN and normal ductal epithelium. For pancreatic cancer, PDAC burden was defined as the volume of PDAC normalized by all PDAC, epithelial ducts, and PanIN total volume of the 3D sample. For each 3D sample, subvolumes were extracted corresponding to all combinations of between 1 and 90 serial tissue images. For each unique combination, the tumor burden of the subvolume was calculated, and the relative error of this burden was determined in relation to the tumor burden of the whole 3D volume. For each 3D sample, measurements were grouped by the number of serial images contained in each subvolume.

Statistical considerations

All significance tests were performed using the Wilcoxon rank sum test. To compare metrics within and between cohorts, median, mean, standard deviation, and interquartile range were determined. Relative error was defined as [measured value – expected value] / expected value. No other statistical calculations were performed in this work.

RESULTS

Construction of cohorts of microanatomically labelled pancreatic tumors

Pancreatic tissues from a total of 71 patients diagnosed with invasive pancreatic ductal adenocarcinoma (PDAC) were analyzed in this work (Fig 1A). Cohorts consisted of individual, pathologist-curated WSIs containing pancreatic cancer from 64 patients ("2D-WSI" cohort, Fig 1B), and serially sectioned histological images of tumor blocks containing pancreatic cancer from seven patients ("3D-CODA" cohort, Fig 1C). As discussed below, Fig. S1 indicates that 64 WSIs in the 2D cohort saturates the tissue composition combinations such that additional images do not provide further heterogeneity information.

For each of these two cohorts, a trained semantic segmentation algorithm was used to label microanatomical components to a lateral resolution of 1 μm. Independent assessment of the trained model revealed an overall accuracy of 93.4% and a minimum per-class precision and recall of 85.6%. For the 3D-CODA cohort, image registration was performed on serially sectioned datasets to create 3D digital tissue volumes (Fig 1B). The minimum number of serial sections per sample was 270 sections (mean: 297 sections, interquartile range: 816 sections). The median reconstructed sample volume was 39.0 mm^3 (mean: 132.2 mm^3, interquartile range: 247.3 mm^3).

Fig 1D displays a local convolution filter applied to the cancer in one 2D WSI and one 3D sample. XY locations with higher PDAC content on the Z (axial) dimension are highlighted, showing greater spatial heterogeneity across planes.. WSIs allow visualization of random, large 2D planes of tumors, and 3D reconstruction of serial sections allows visualization of complex intra-tumoral heterogeneity and 3D cancer morphology. Large volume maps of pancreatic cancer tissue enable the quantification of spatial relationships among cells that may be missed in the much smaller-sized regions of 3D organs that are sampled by TMAs and individual WSIs (Fig 1E).

Comparison of intra-tumoral and inter-tumoral heterogeneity in microanatomical composition

We sought to quantify the relationship between inter-tumoral differences in tissue content, as measured in the 2D-WSI cohort, and corresponding intra-tumoral differences in tissue content, as measured in the 3D-CODA cohort. First, we determined the per-tissue component composition of each image in the 2D-WSI and 3D-CODA cohorts using CODA. The tissue components segmented by CODA in the 2D-WSI and 3D-CODA cohorts included PDAC, non-neoplastic ductal epithelium, islet of Langerhans, blood vessel, extracellular matrix (ECM), acini, fat, extracellular matrix (ECM), and nerve. To minimize sample-size bias for this calculation, any 3D-CODA sample that contained >64 serial sections was randomly subsampled to 64 consecutive sections. Next, we analyzed the range in tissue content for each of the tested tissue component in the 64 samples of 2D-WSI cohort and for each of the samples where that component was present in the 3D-CODA cohort (Fig 2A). To account for the arbitrariness of our sampling of the seven 3D samples of pancreatic cancer, we subsampled the 3D cohorts to all possible combinations of one through seven samples. These data revealed that the wide distribution in tissue content present in 64 independent WSIs (one per patient) was nearly fully represented by the heterogeneity of the seven 3D samples. Besides nerve, the inter-patient heterogeneity in each tissue component of the 2D-WSI cohort was statistically insignificant when compared to the interpatient-heterogeneity of the seven 3D-CODA samples (Fig 2B).

This analysis revealed that the range in heterogeneity observed in just three 3D samples was necessary to cover the full range of intra-patient heterogeneity in tissue composition (exceed a p-value of 0.05) (Fig 2C). The occurrence of PDAC tissues present in the 2D-WSI cohort was compared to that of all combinations of samples present in the 3D-CODA cohort to assess statistical significance of the overlap between the two cohorts (Fig S1A).

Finally, to validate the number of WSIs in the 2D-WSI cohort, we calculated the heterogeneity in tissue composition for various numbers of WSIs. This analysis measured the number of 2D WSIs necessary to saturate in inter-patient compositional heterogeneity. We found that composition saturates at 40-50 slides (Fig S1), justifying our use of 64 WSIs in this work.

The rapid decay in spatial correlation in tissue composition within pancreatic tumors

We asked how much would spatial resolved tissue composition measured in serial sections change when traveling in a straight line through a 3D tumor. To determine the correlation length of each pancreatic tissue component (PDAC, fat, etc.) within 3D pancreatic tumors – i.e. the persistence distance over which the tissue composition remained significantly correlated – we calculated the spatial (pixel to pixel) correlation of structures across the samples of the 3D CODA cohort. This correlation was calculated for each tissue component and for all whole-slide images spaced between 4 μm and 720 μm apart in the 3D samples. Correlation was averaged across the seven 3D samples and plotted as a function of distance between slides (Fig 3A). This assessment was repeated for the eight main tissue components present in the pancreatic microenvironment (Fig 3A).

This analysis determined the extent to which each tissue maintains anatomical continuity and structural organization. Our analysis of each individual tissue revealed that more abundant tissue structures in the pancreatic tumor tissues, such as ECM and acini were spatially correlated over large distances within the blocks, requiring >180 slides (or 720 μm) until they reached a spatial correlation that had decreased by >50%. For sparser tissues such as nerve and blood vessel, no more than a distance of 60 μm, corresponding to five 4-μm-thick slides, were required for the spatial correlation in the content in that tissue component to fall below <50% (Fig 3B). This highlights the significant changes that occur in tissue structures across short distances. A corollary of this is that sampling a 3D tumor at a rate larger than the correlation length is insufficient for a rigorous assessment of the spatially resolved composition of that tumor. This provides guidelines for the minimum spatial rate (maximum distance between whole slides) at which the content in a specific tissue component needs to be assessed.

The limited utility of TMAs to assess of tumor heterogeneity in tissue composition

To further quantify the loss in spatial correlation of the PDAC component across thick slabs of tissue, we created virtual cores within the large 3D samples to simulate TMAs. In specimens of the 3D-CODA cohort, 50 locations were manually chosen on the first H&E image as regions containing visually high composition of cancer. This is to mimic how tumor TMA cores, guided by an expert pathologist, are typically produced from a columnar tumor sample (or biopsy). Virtual columnar cores were taken at each chosen coordinate, and virtual TMA slices (vTMAs) were generated along these columnar cores (Fig 4A). For each core, we quantified the error in PDAC composition between the first section of the core and any other given section

(Fig 4B) Assessing the average of this error across 50 virtual cores (Fig 4C), we found that the relative error increases dramatically within distances as low as 1.2 mm (240 tissue 4-μm sections). The mean relative error in cancer composition increases beyond 15% after 150 sections. We note that tissue composition of tissue cores changes rapidly after merely tens of histological sections.

Hundreds of TMAs are needed to capture the true tissue composition of WSIs and 3D tumors

We next aimed to understand the amount of information lost when subsampling a heterogeneous 3D tumor sample with a WSI or a TMA core of 1 mm in diameter instead of a full 3D assessment. To do this, we simulated virtual TMA cores (vTMAs) randomly located in the 2D WSIs and within the 3D-CODA samples. We quantified the number of randomly sampled, non-overlapping vTMAs necessary to estimate the tissue composition of individual whole slide images within a preset error. For each simulation, between one and 100 vTMAs were generated, and the cumulative composition of eight microanatomical components of the pancreas (PDAC, fat, blood vessel, etc.) as well pancreatic intraepithelial neoplasms (PanIN) were compared to the overall content of these components of the WSI. This process was repeated for WSIs from all 64 individuals in the 2D-WSI cohort, and the resulting errors per simulation plotted as a function of the number of TMAs sampled (Fig 5A). This process was also repeated to estimate the resulting errors per simulation as function of vTMAs within the seven 3D-CODA volumes (Fig 5B), and the error when using randomly sampled, non-overlapping virtual WSIs within the seven 3D-CODA volumes (Fig 5C).

For each simulation, increasing the number of TMAs for the rigorous assessment of bulk tissue composition in 2D images (Fig. 5A) and 3D samples (Fig. 5B) or WSIs for 3D samples (Fig. 5C), decreased the error of estimation of tissue composition, as expected. The number of simulated TMAs or WSIs necessary to reach pre-set error rates varied across different microanatomical tissue components of the pancreas. The number of TMAs or WSIs necessary to reach <10% error in estimation of true WSI or 3D-volume composition enabled the identification of low-heterogeneity and high-heterogeneity components of low- and high-heterogeneity (Fig 5D). ECM consistently showed the lowest heterogeneity, with an average of 84 TMAs necessary to reach <10% error in the estimation of 2D WSI composition, an average 479 TMAs necessary to reach <10% error in the estimation of 3D-volume composition, and an average 19 WSIs necessary to reach <10% error in the estimation of 3D-volume composition. In contrast, accurate estimation of cancer composition required significantly more TMAs. The estimation of content in nerves and PanINs revealed that these tissue components were the less prevalent, which required 100TMAs for <10% error in estimation of 2D WSI composition, >700 TMAs (for nerves) and 800 TMAs (for PanIN) for <10%error in estimation of 3D-volume composition.

Required sampling in 3D samples depends on the relative prevalence of the target tissue

Here, we assess the relationship between the sampling in a 3D tissue necessary to reach a preset error in the estimation of PDAC content and the relative content of PDAC and cancer precursor lesions PanIN in that tissue. For this calculation, we first utilized a previously reported cohort of 48 large 3D reconstructed samples of human pancreas tissue containing PanINs.[5] We defined PanIN burden as the volume percent of PanIN within the pancreatic ductal system: P_{burden} = volume of PanIN / (volume of PanIN + normal ductal epithelium). Next, we calculated P_{burden} for all possible combinations of consecutive slides subsampled

from the above 3D cohort and calculated the relative error of the subsampled region to the P_{burden} of the full 3D sample (Fig 6A). Visualizing this as bar plots for low, medium, and high P_{burden} ($0< X \leq 33\%$, $33\%< X \leq 66\%$, and $66\%< X \leq 100\%$, respectively) revealed that few slides are needed to accurately determine the neoplastic content of samples containing large fractions of PanIN, while many slides are needed to accurately determine the neoplastic content of samples containing low fractions of PanIN (Fig 6B) revealed that for samples.

After validating the PanIN burden calculation on the cohort of 48 adjacent healthy tissue blocks, the same calculation was computed for the PDAC burden on the initial seven 3D-CODA blocks obtained from individuals diagnosed with pancreatic cancer. We defined an analogous cancer burden: C_{burden} = volume of cancer / (volume of cancer + volume of PanIN + volume of normal ductal epithelium). Again, we found that few slides are needed to estimate the composition of cancer in samples with high cancer burden, but that many slides are necessary to estimate cancer composition in samples with sparse cancer cells (Fig 6C).

These results suggest the rather intuitive guideline that the rarer the tissue component (e.g. PDAC content in samples from patients with low PDAC burden) to be studied is, the larger the number of WSIs is required for a rigorous assessment of that component content.

DISCUSSION

Methods for spatially resolved cellular profiling has enabled in-depth quantitative mapping of tissues and tumors to study inter-patient and intra-patient differences in normal human anatomy and disease onset and progression. These methods profile extremely limited regions, which may impact the evaluation of tissue content and local heterogeneity due to tissue sub-sampling**.** Here, we apply CODA, a deep learning-based tissue mapping platform, to reconstruct the 3D microanatomy of surgically resected human pancreas specimens taken from individuals diagnosed with pancreatic cancer. To compare differences in the inter- and intra-tumoral heterogeneity in tissue content, we assess the tissue composition of a cohort of two-dimensional (2D) whole slide images (WSIs), and a cohort of 3D serially sectioned and reconstructed tissues of pancreata using CODA. We demonstrate the value of using 3D as the gold standard, by analyzing information loss and sampling issues when using WSIs and TMAs.. The spatial correlation in microanatomical tissue content decays significantly within a span of just a few microns within tumors. As a corollary, hundreds of TMAs and tens of WSIs are required to estimate bulk tumor composition with <10% error in any given pancreatic tumor. The large error in the estimation of the occurrence of rare tissue components, for examples the PDAC content in the tumor of a patient with a low PDAC burden or the PanIN content in the pancreas of a patient with a low PDAC burden, requires large numbers of WSIs to rigorously detect and measure these tissue components. While 2D assessments using WSIs are typically sufficient for clinical diagnostic, they are insufficient for accurate assessments of spatially resolved tissue component composition analysis of organs and diseased tissues. A consequence is that digital pathology done on whole slides, which presumes that intra-organ variations in cellular content are smaller than patient-to-patient organ variations, may lead to erroneous conclusions, even in organs that are believed to be highly homogenous like the lung. In sum, we demonstrate that 3D assessments are necessary to accurately assess tissue composition, tumor burden and provide guidelines for the rate of sampling necessary to rigorously assess spatially resolved tissue composition and associated tissue density and intercellular distances.

REFERENCES

1. Liu, Y. *et al.* High-Spatial-Resolution Multi-Omics Sequencing via Deterministic Barcoding in Tissue. *Cell* **183**, 1665-1681.e18 (2020).
2. Ozsolak, F. & Milos, P. M. RNA sequencing: advances, challenges and opportunities. *Nat Rev Genet* **12**, 87–98 (2011).
3. Pidsley, R. *et al.* Critical evaluation of the Illumina MethylationEPIC BeadChip microarray for whole-genome DNA methylation profiling. *Genome Biol* **17**, 208 (2016).
4. Cheng, M., Bhujwalla, Z. M. & Glunde, K. Targeting Phospholipid Metabolism in Cancer. *Front. Oncol.* **6**, (2016).
5. Braxton, A. M. *et al. Three-dimensional genomic mapping of human pancreatic tissue reveals striking multifocality and genetic heterogeneity in precancerous lesions*. http://biorxiv.org/lookup/doi/10.1101/2023.01.27.525553 (2023) doi:10.1101/2023.01.27.525553.
6. Bell, A. T. F. *et al. PanIN and CAF Transitions in Pancreatic Carcinogenesis Revealed with Spatial Data Integration*. http://biorxiv.org/lookup/doi/10.1101/2022.07.16.500312 (2022) doi:10.1101/2022.07.16.500312.
7. Vogelstein, B. *et al.* Cancer Genome Landscapes. *Science* **339**, 1546–1558 (2013).
8. Lin, J.-R., Fallahi-Sichani, M. & Sorger, P. K. Highly multiplexed imaging of single cells using a high-throughput cyclic immunofluorescence method. *Nat Commun* **6**, 8390 (2015).
9. Angelo, M. *et al.* Multiplexed ion beam imaging of human breast tumors. *Nat Med* **20**, 436–442 (2014).
10. Goltsev, Y. *et al.* Deep Profiling of Mouse Splenic Architecture with CODEX Multiplexed Imaging. *Cell* **174**, 968-981.e15 (2018).
11. Kuett, L. *et al.* Three-dimensional imaging mass cytometry for highly multiplexed molecular and cellular mapping of tissues and the tumor microenvironment. *Nat Cancer* **3**, 122–133 (2021).

12. Eng, C.-H. L. *et al.* Transcriptome-scale super-resolved imaging in tissues by RNA seqFISH+. *Nature* **568**, 235–239 (2019).

13. Xia, C., Fan, J., Emanuel, G., Hao, J. & Zhuang, X. Spatial transcriptome profiling by MERFISH reveals subcellular RNA compartmentalization and cell cycle-dependent gene expression. *Proc. Natl. Acad. Sci. U.S.A.* **116**, 19490–19499 (2019).

14. Fischer, A. H., Jacobson, K. A., Rose, J. & Zeller, R. Hematoxylin and Eosin Staining of Tissue and Cell Sections. *Cold Spring Harb Protoc* **2008**, pdb.prot4986 (2008).

15. De Matos, L. L., Trufelli, D. C., De Matos, M. G. L. & Da Silva Pinhal, M. A. Immunohistochemistry as an Important Tool in Biomarkers Detection and Clinical Practice. *Biomark Insights* **5**, BMI.S2185 (2010).

16. Li, Q. K. *et al.* Neoplastic cell enrichment of tumor tissues using coring and laser microdissection for proteomic and genomic analyses of pancreatic ductal adenocarcinoma. *Clin Proteom* **19**, 36 (2022).

17. Susaki, E. A. *et al.* Whole-Brain Imaging with Single-Cell Resolution Using Chemical Cocktails and Computational Analysis. *Cell* **157**, 726–739 (2014).

18. Hong, S.-M. *et al.* Three-dimensional visualization of cleared human pancreas cancer reveals that sustained epithelial-to-mesenchymal transition is not required for venous invasion. *Modern Pathology* **33**, 639–647 (2020).

19. Kiemen, A. L. *et al.* CODA: quantitative 3D reconstruction of large tissues at cellular resolution. *Nat Methods* **19**, 1490–1499 (2022).

20. Koyuncu, C. *et al.* Visual Assessment of 2-Dimensional Levels Within 3-Dimensional Pathology Data Sets of Prostate Needle Biopsies Reveals Substantial Spatial Heterogeneity. *Laboratory Investigation* **103**, 100265 (2023).

21. Liu, J. T. *et al.* Engineering the future of 3D pathology. *The Journal of Pathology CR* cjp2.347 (2023) doi:10.1002/cjp2.347.

22.Crawford, A. J. *et al. Precision-engineered biomimetics: the human fallopian tube*. http://biorxiv.org/lookup/doi/10.1101/2023.06.06.543923 (2023) doi:10.1101/2023.06.06.543923.

23.Kiemen, A. L. *et al.* Tissue clearing and 3D reconstruction of digitized, serially sectioned slides provide novel insights into pancreatic cancer. *Med* **4**, 75–91 (2023).

24.Kiemen, A. L. *et al.* Intraparenchymal metastases as a cause for local recurrence of pancreatic cancer. *Histopathology* **82**, 504–506 (2023).

25.Fujikura, K. *et al.* Intraductal pancreatic cancer is less responsive than cancer in the stroma to neoadjuvant chemotherapy. *Modern Pathology* **33**, 2026–2034 (2020).

26.Chen, L.-C., Papandreou, G., Kokkinos, I., Murphy, K. & Yuille, A. L. DeepLab: Semantic Image Segmentation with Deep Convolutional Nets, Atrous Convolution, and Fully Connected CRFs. (2016) doi:10.48550/ARXIV.1606.00915.

Data availability statement

The data analyzed here is available from the corresponding author upon request

Author contributions

A.L.K. and D.W. conceived the project. A.L.K. A.M.B., K.F., T.C., S.H., and R.H.H. collected and processed the human pancreas samples. A.L.K., A.F., E.V, S. J, V.M.R, A.J., and P.W. conducted the image analysis and heterogeneity quantifications. S.M, L.W, and R.H.H. validated histological analysis as clinical experts in pancreatic cancer pathology. A.F., A.L.K., and D.W. wrote the first draft of the manuscript, which all authors edited and approved.

Figures and Captions

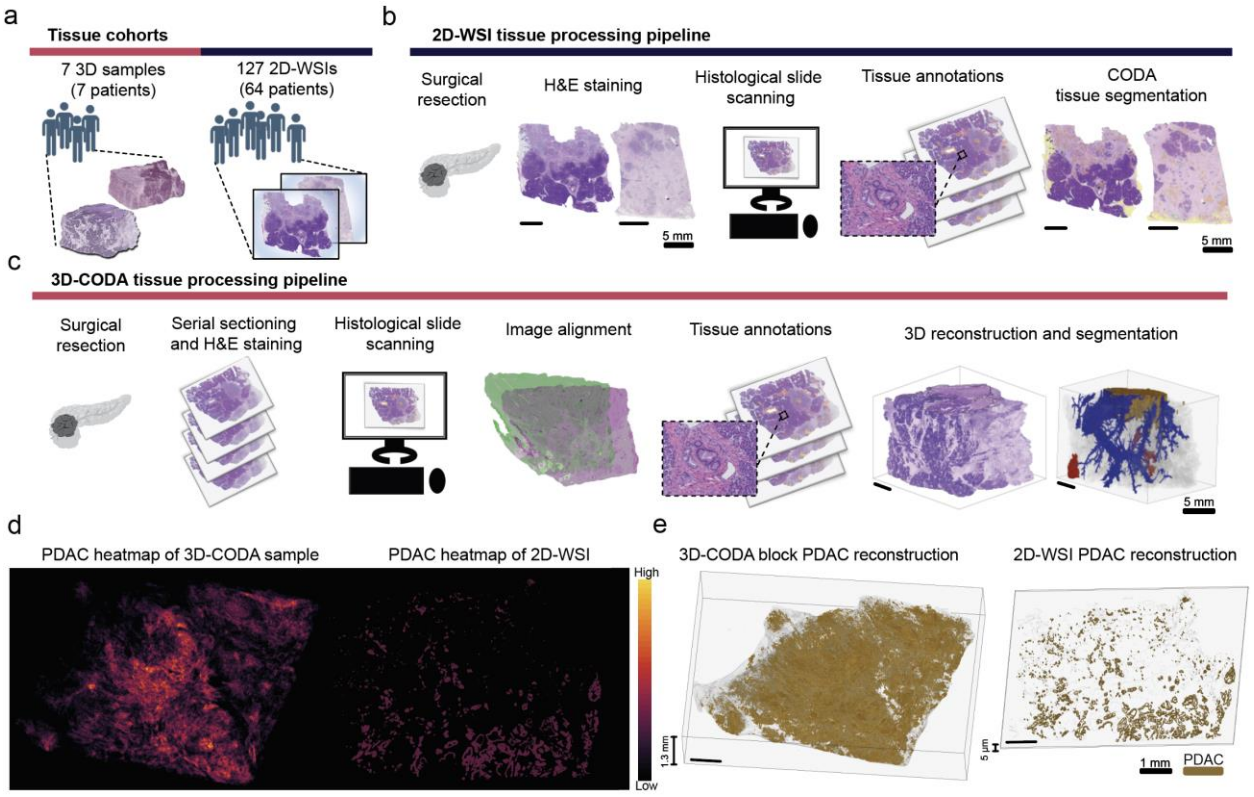

Fig. 1. Construction of cohorts of microanatomically labelled pancreatic cancer histological sections for assessment of inter- and intra-patient tumor heterogeneity. (**a**) Cohorts of 3D blocks and 2D-WSIs from surgically resected human pancreatic tissues were retrospectively collected from 71 individuals diagnosed with pancreatic cancer. A cohort of 127 specimens from 64 different patients were analyzed as single whole slide ("2D-WSI" cohort; 1-2 slides per patient). A cohort of 7 blocks were serially sectioned and reconstructed in 3D using the AI-based platform CODA ("3D-CODA" cohort). (**b**) For the processing of the 2D-WSI cohort, resected tissues were histologically sectioned, stained with H&E and digitized. CODA segmentation was used to label 10 different microanatomical components (including epithelial ducts, fat, islets of Langerhans, PDAC, acini, nerves, blood vessels, and extracellular matrix (ECM)) at a resolution of 1 micron. (**c**) For the processing of the 3D-CODA cohort, specimens were serially sectioned, H&E-stained, digitized and registered into aligned tissue volumes. Manual annotations of a subset of images were used to train a deep learning model to automatically segment anatomical labels and subsequently reconstructed them in 3D. (**d**) Local PDAC content projected in 2D from a stack of 127 sections shown as a heatmap, which exemplifies the spatial distribution of PDAC tissue content in that block (left) and associated heatmap from a single whole slide. Higher PDAC content on the z-axis is highlighted in yellow regions and low PDAC content is labelled in black regions. (**e**) 3D reconstruction of the PDAC content shown in panel (d), which highlights the difference in tissue structural connectivity and spatial distribution measured in a 3D block vs. a single whole slide.

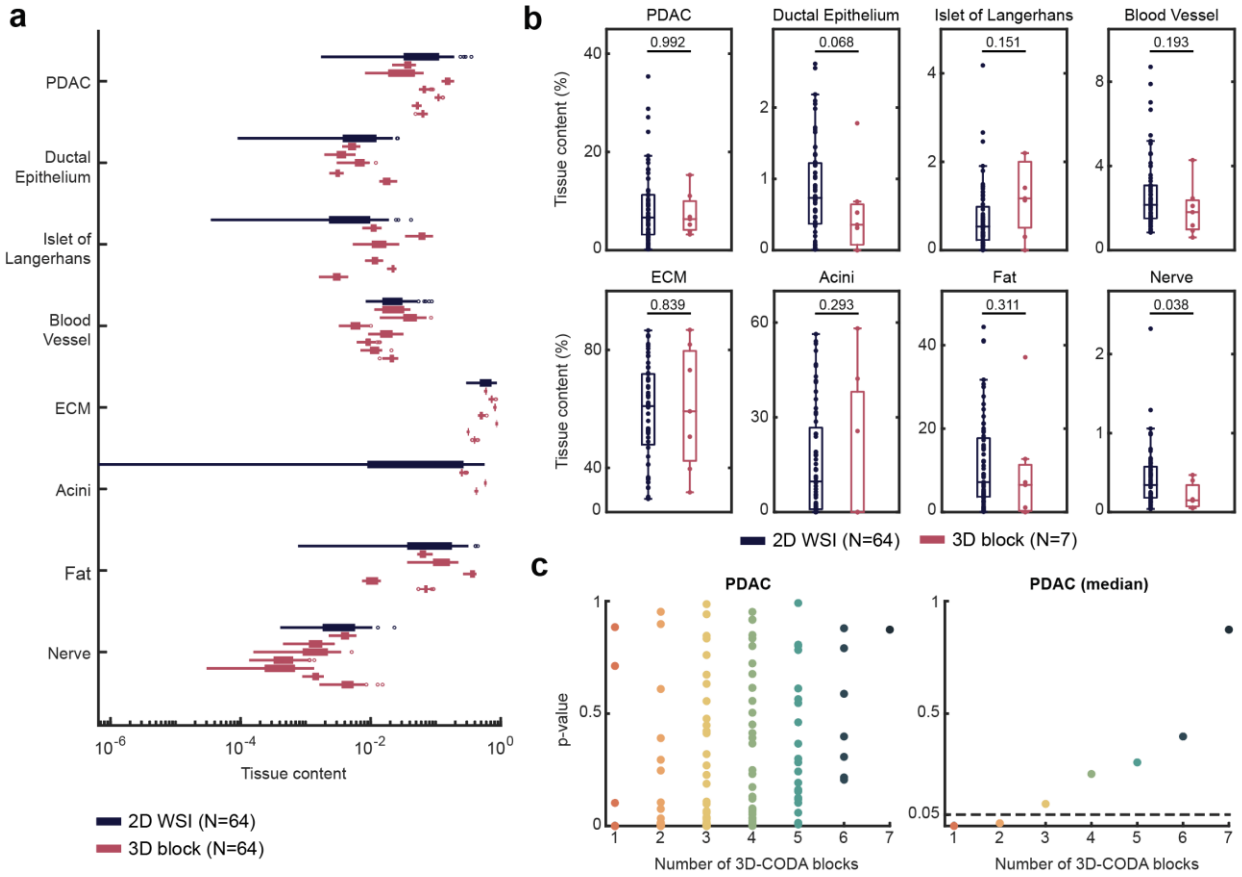

Fig. 2. **Comparison between inter- and intra-patient tumoral heterogeneity in tissue composition**. (**a**) Range in bulk tissue content for 64 slides from the 2D-WSI cohort (black) and the 7 samples (each containing 64 slides) of the 3D-CODA cohort (red). The tissue components segmented and analyzed by CODA for both cohorts include PDAC, ductal epithelium, islet of Langerhans, blood vessel, extracellular matrix (ECM), acini, fat, and nerve. Note that tissue components are not all present in all 7 blocks, which is why the number of blocks shown is different for different tissue components. (**b**) Comparison between the percent of each tissue component for each section of the 2D-WSI cohort and for the blocks of the 3D-CODA cohort. This reveals non-significant differences in inter- and intra-patient tumoral heterogeneity between the two cohorts across all tested tissue components, besides nerve. (**c**) 2D-WSI tissue composition range is compared to 3D-CODA composition range for all possible combinations of one through seven 3D samples (left panel), revealing that the median difference between the 2D and 3D cohorts become non-significant ($p>0.05$) with as few as three 3D samples (right panel).

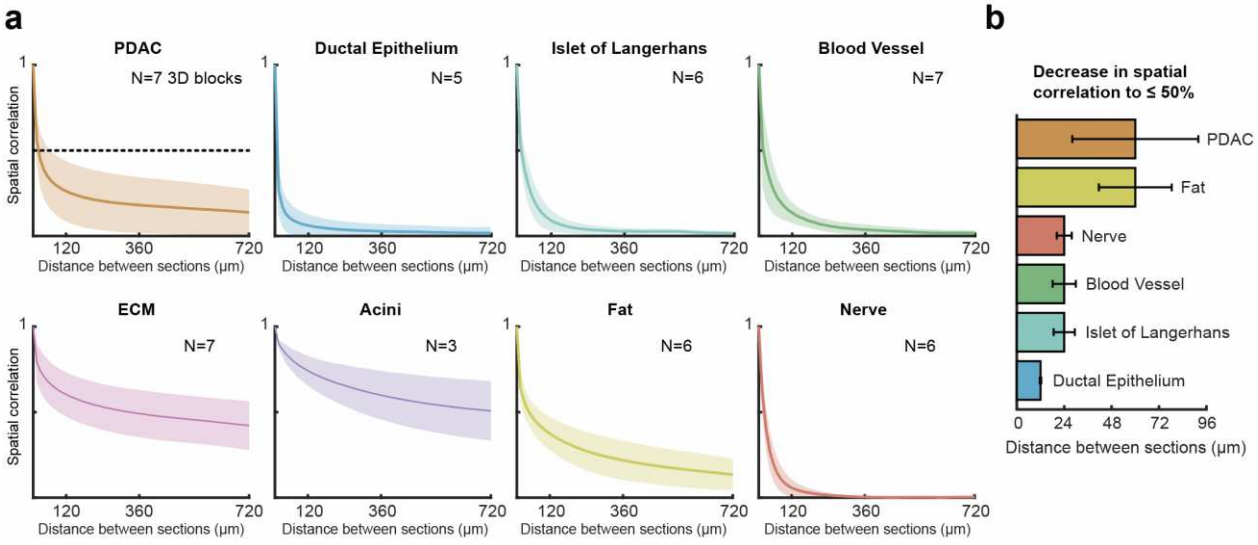

Fig. 3. Rapid decay of the spatial correlation in tissue content within tumors. (**a**) 2D spatial correlation in tissue content was calculated for all combinations of pairs of sections within the samples of the 3D-CODA cohort. For each tissue type, the correlation was plotted as a function of the distance between the section pairs. Dotted black line shows a correlation of 50%. Dark line is the mean; shaded area is the standard deviation. As tissue components are not all present in all 7 blocks, the number N of blocks shown is different for different tissue component. (**b**) Distances at which the correlation falls below 50% for each of the test tissue components and each of the 7 samples in the 3D-CODA cohort. This shows the tissue composition in a given section in a block becomes essentially uncorrelated with tissue composition in a second slide in the same block if that slide is just tens of microns from the first one. In other words, the prevalence in composition in a PDAC tumor is extremely short.

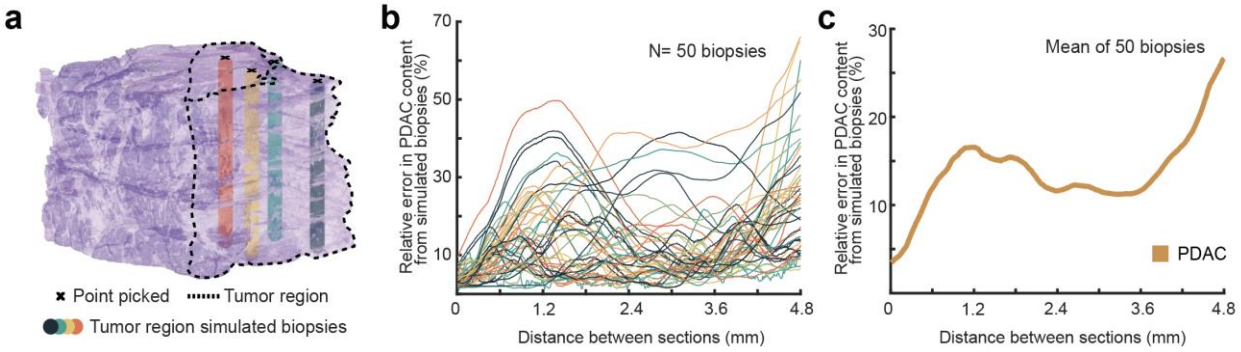

Fig. 4. Error when TMA cores are used to assess spatial tissue content in a tumor. (**a**) To simulate a pathologist-guided selection of TMA cores from virtual columnar cores ("biopsies"), 50 target regions containing cancer were manually selected from the top slide for each of a block. (**b**) Virtual TMA (vTMAs) cores were obtained from the columnar cores, and the relative error in PDAC content between the top section and each vTMA was calculated. (**c**) Ensemble-averaged relative error in PDAC content for the 50 biopsies. The content in PDAC changes significantly along the biopsies.

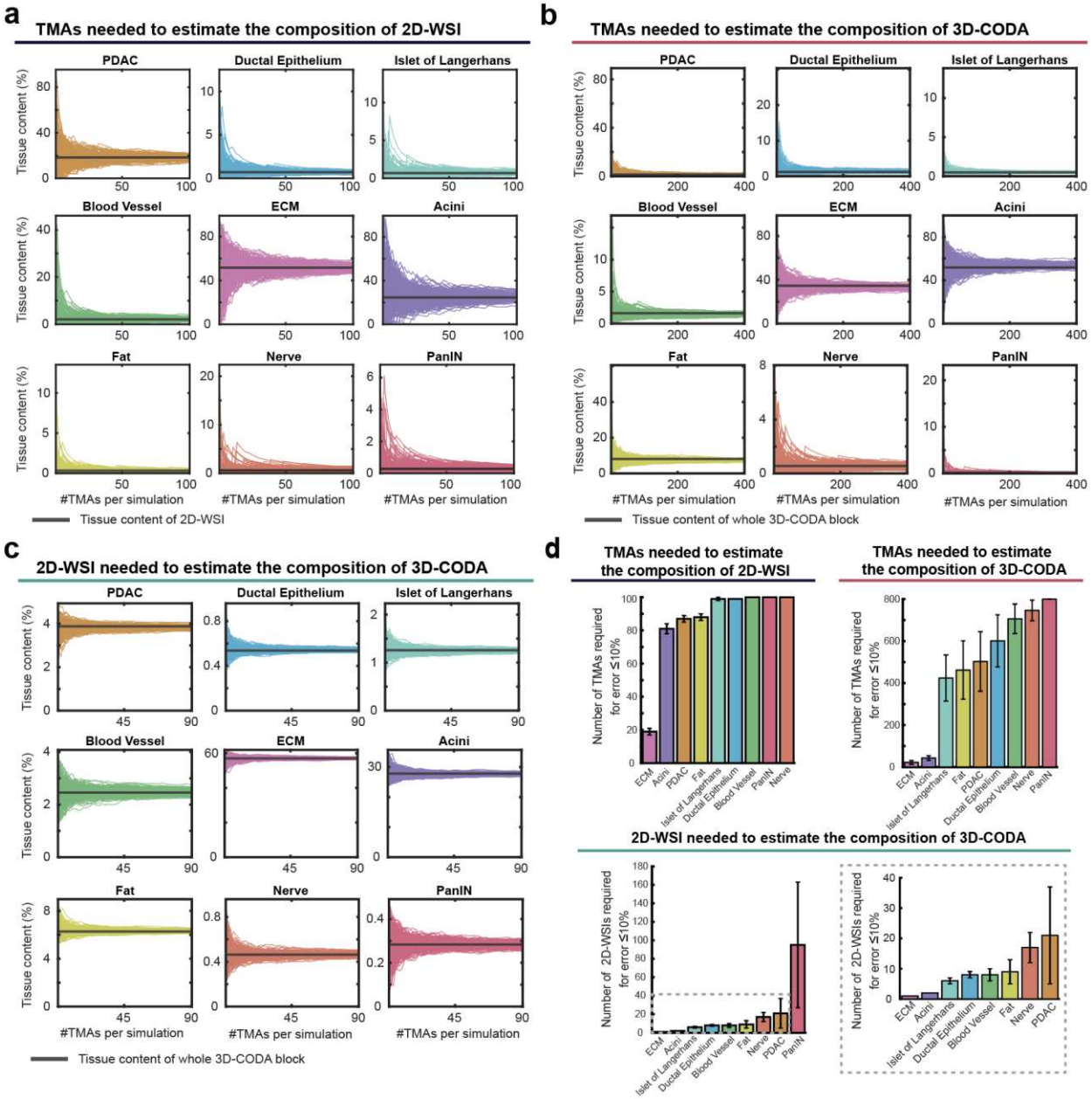

Fig. 5. Hundreds of TMAs and tens of WSIs are needed to accurately estimate the true bulk tissue composition of 3D tumors. (**a**) The loss in the accuracy of calculation of tissue composition due to TMA subsampling was measured through 200 simulations of 1 to 100 virtual TMAs (vTMAs) in the 2D-WSI cohort. Tissue composition of the generated vTMAs was compared to the average 2D-WSI (black line). (**b**) The calculation of (a) was repeated for calculation of the loss in accuracy of estimation of tissue composition between TMAs (from 1 to 400 virtual TMAs) and 3D tumors. (**c**) The calculation of (a) was repeated for calculation of the loss in accuracy of estimation of tissue composition using actual WSIs and 3D tumors (of 1 to 90 actual WSIs). (**d**) Distilling the information from the simulations shown in (a-c), we calculated the number of TMAs and WSIs necessary to estimate WSI and 3D-tumor composition with ≤10% error. ECM showed the lowest error across all simulations, while sparser components, such as blood vessels, nerves, and PanIN required more (tens to hundreds) of tissue sections to reach ≤10% error.

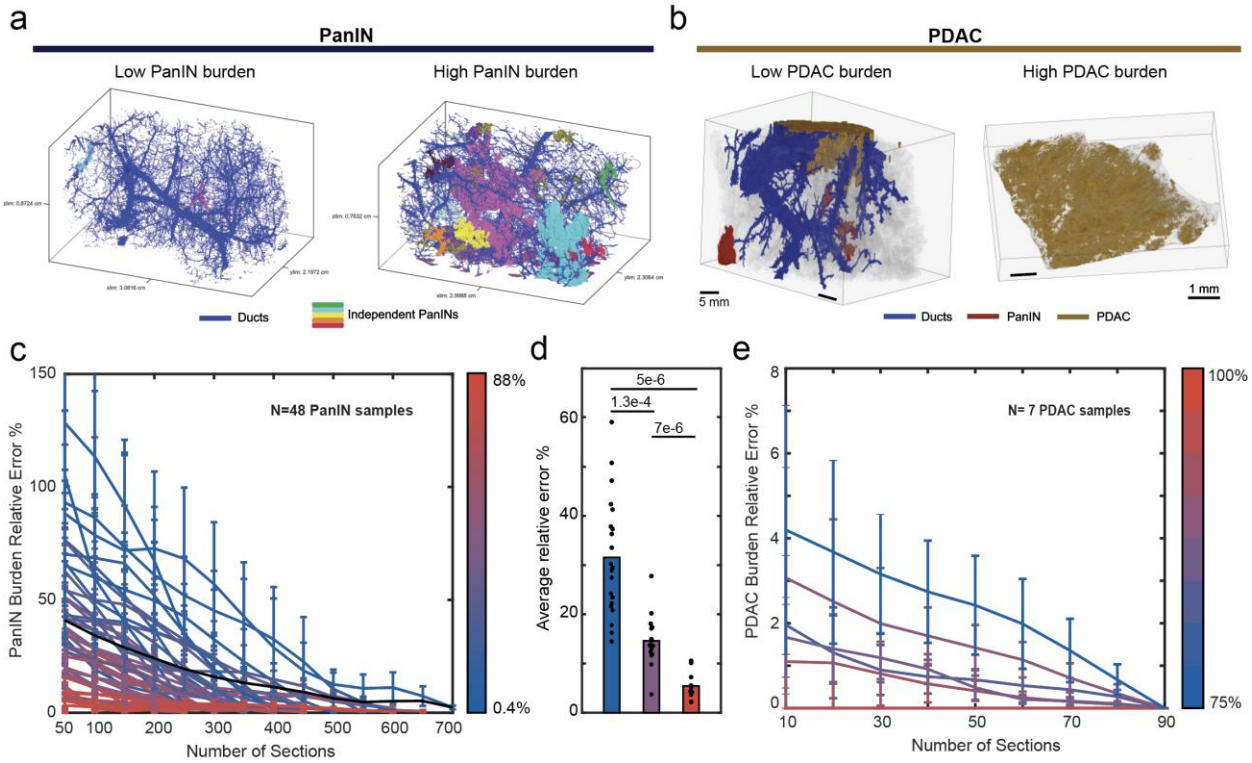

Fig. 6. The number-of-WSIs-needed to capture the true bulk incidence in pancreatic neoplasms depends on their frequency in the sample. (**a and b**) 3D rendering of pancreata that contain low and high PanIN burden (**a**) and low and high PDAC burden (**b**). (**c**) For 48 3D pancreata containing PanIN (precursors to pancreatic cancer), the error in estimation of overall PanIN burden as a function of the number of consecutive sections subsampled was computed. Lines are color-coded according to the overall PanIN burden of the sample, from low (blue) to medium (purple) to high (red). (**d**) The data in (c) binned according to overall PanIN burden to show that fewer sections are needed to accurately estimate the PanIN burden of samples that contain many PanIN lesions, and *vice versa*. (**e**) The calculation of (c) was repeated for the seven samples containing PDAC in the 3D-CODA cohort to show that fewer sections are needed to accurately estimate cancer content in samples that contain high cancer composition, and *vice versa.*

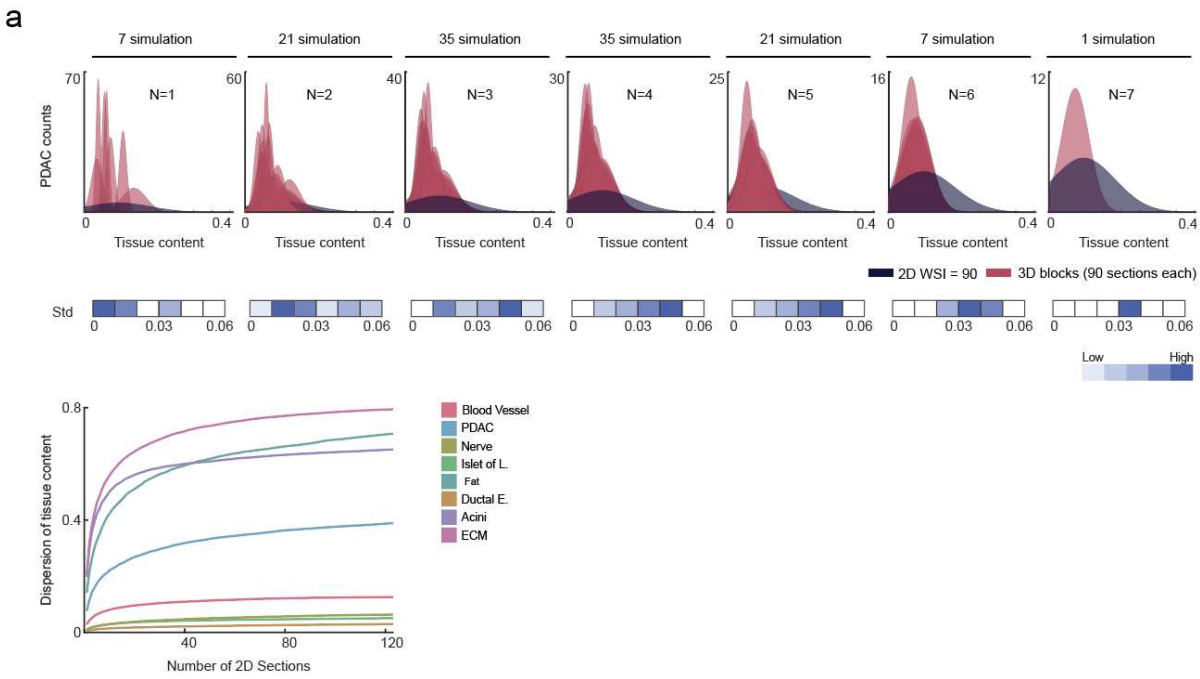

Fig. S1. Number of patients necessary to capture the full range in tissue composition of PDACs. (**a**) Distributions in PDAC content for all combinations of individual 3D samples (red) compared to the full range in PDAC composition shown by the 64 patients (blue) in the 2D-WSI cohort. N is the number of 3D samples used in each plot. (**b**) Number of 2D WSIs (i.e. number of patients represented by one slide) necessary to saturate in inter-patient compositional heterogeneity.. Composition curves saturate at ~40-50 sections, justifying the number of 2D slides used for the 2D WSI cohort.